AB FOCAL VELOCITY ANALYSIS

SIYAVASH TORABI[1], ABDORAHIM JAVAHERIAN[1,2] and MAJID NABI-BIDHENDI[1]

1 Institute of Geophysics, University of Tehran, Iran. javaheri@ut.ac.ir
2 Department of Petroleum Engineering, Amirkabir University of Technology, Tehran, Iran.

(Received July 1, 2013; revised version accepted February 26, 2014)

ABSTRACT

Torabi, S., Javaherian, A. and Nabi-Bidhendi, M., 2014. *AB* focal velocity analysis. *Journal of Seismic Exploration*, 23: 153-175.

A conventional semblance velocity analysis is an analysis in which it is assumed that there is no amplitude-variation-with-offset (AVO) on a hyperbolic event in an input CMP gather. As a result, events with a strong AVO anomaly, especially the ones with polarity reversal, will not produce a sharp semblance attribute. Such an AVO anomaly can be seen from the top of some class 1 and class 2 sands. To overcome this disadvantage, data modeling with amplitude variation expressed by an intercept and gradient *AB* semblance was introduced. On the other hand, an *AB* semblance has a resolution approximately twice as low as that of the conventional semblance.

In this study, a new method called the *AB* focal velocity analysis (*AB*-FVA) was introduced as a tool for high resolution velocity analysis in the presence of class 2 AVO. In this method, a velocity analysis is run in the focal domain to achieve a higher resolution. The *AB*-FVA was introduced by combining the *AB* semblance and the focal velocity analysis (FVA). The *AB*-FVA uses the same explicit formula for the generalized semblance attribute as used in the *AB* semblance. Two synthetic CMP datasets were used to demonstrate an improvement in the velocity analysis by *AB*-FVA in comparison with the *AB* semblance and the other two methods (the FVA and the semblance). The assessment of these four methods over synthetic datasets proved that the *AB*-FVA has the least smearing along time and velocity directions compared to other methods. Also, two real datasets were used to check the quality of the velocity analysis by the *AB*-FVA compared to the other three methods. The first dataset was a deep marine CMP gather containing strong long period multiples. The second dataset was a shallow part of a CMP gather showing class 2 AVO. By comparison of the results obtained from synthetic and real datasets it was concluded that *AB*-FVA was a promising method for velocity analysis.

KEY WORDS: seismic velocity analysis, *AB* focal velocity analysis (*AB*-FVA), focal transform, *AB* semblance, semblance, class 2 AVO.

0963-0651/14/$5.00

INTRODUCTION

Semblance (Neidell and Taner, 1971) is the most common method in velocity analysis in reflection seismology. While effective in most practical situations, semblance becomes troublesome in the case of variation of amplitudes along seismic events (Sarkar et al., 2001). The main reason for this pitfall is based on the assumption that the wavelet amplitude does not vary with the offset. Thus, in the case that strong amplitude-variation-with-offset (AVO) appears in data the results of a semblance are not reliable. The extreme case of such phenomena is in class 1 and class 2 sands polarity reversals (Rutherford and Williams, 1989). Avoiding such pitfalls can be achieved by taking the AVO effects into account. Such optimization should improve a velocity analysis as well as the normal move out (NMO) corrections and also the determination of prestack AVO attributes. Some methods have been developed to overcome these semblance pitfalls for AVO analysis.

Eigenvalue methods (e.g., Biondi and Kostov, 1989; Key and Smithson, 1990) use the fact that the signal covariance matrix is of a low rank in the absence of noise. High-resolution spectral estimates are rather sensitive to the estimates of covariance matrices, which in seismic applications need to be obtained from only a few data samples in time. Also by incorporation of AVO, even for complex variations this method can be converted to an AVO-friendly method. The differential semblance method (e.g., Symes and Kern, 1994) works by comparing each trace with traces of similar offsets. Because it compares only traces of similar offsets, this method is less sensitive to AVO variations than the traditional semblance analysis. Recently, Sarkar et al. (2001, 2002) have developed *AB* semblance algorithms to correct the semblance measurement for amplitude variations. Fomel (2009) shows the semblance attribute as a correlation with a constant and derives an explicit mathematical expression for the measure that corresponds to a correlation with an amplitude trend. This expression is equal to the *AB* semblance. Although *AB* semblance produces an AVO friendly velocity panel, the *AB* measurement is generally twice as sensitive to noise and has a resolution twice lower compared with the semblance (Fomel, 2009). The FVA (Torabi and Javaherian, 2010) was introduced as a high resolution velocity analysis method. This method uses a focal domain as the domain for velocity analysis. Small differences in the velocity of an event in the t-x domain will cause a large effect in the focal domain. In this paper, a new method of velocity analysis will be introduced that is a combination of a focal transform velocity analysis and an *AB* semblance. Using a focal transform as the domain for velocity analysis will result in a higher resolution and better accuracy in comparison with the semblance method (Torabi et al, 2013). Also, using a generalized equation of semblance in the focal domain will result in a high-resolution AVO friendly velocity analysis (*AB*-FVA). Similar to the other high-resolution methods, a higher resolution can be obtained by a higher computational cost. Meanwhile, powerful computers that are available in most

processing centers make the computational cost less important given the resolution that can be achieved. In this paper, after a brief review of the *AB* semblance and the focal transform equations of Berkhout et al. (2004), the methodology of *AB*-FVA velocity analysis will be discussed. This method was tested on synthetic and real datasets to check the ability of this method and to evaluate the ability of *AB*-FVA in a velocity analysis in comparison with three other methods.

METHODOLOGY

AB Semblance

Fomel (2009) considers the conventional semblance attribute as a correlation with a constant and defines *AB* semblance as a correlation with a trend. The trend that is used in the *AB* semblance is an expression of the PP reflection coefficient in Shuey's approximation (Shuey, 1985)

$$b_i = A + B\phi_i \quad , \tag{1}$$

where b_i is the reflection coefficient of an event (NMO corrected) along the offset, A and B are the AVO intercept and gradient, respectively, and ϕ_i is $\sin^2\theta_i$ with θ_i corresponding to the reflection angle at a trace i.

The normalized correlation coefficient of the two series of numbers can be generally defined as:

$$\gamma(\mathbf{a},\mathbf{b}) = \mathbf{a}\cdot\mathbf{b}/|\mathbf{a}|\cdot|\mathbf{b}| \quad , \tag{2}$$

where **a** and **b** are the two series of numbers and γ is the correlation coefficient of these two series. Using Shuey's approximate equation [eq. (1)], a relationship between the offset and reflection angle can be defined. On the other hand, A and B from the least-squares fitting of the trend can be estimated. These estimated equations can be differentiated with respect to A and B. Setting the derivatives to zero, and solving a system of two linear equations produces the desired linear equations. Having A and B from the least-squares equations and substituting them into the correlation coefficient equation [eq. (2)] and squaring the results leads to a new measurement which corresponds to the definition of semblance using a normalized least-squares method by Sarkar et al. (2001). Therefore, the generalized semblance measurement (α) is defined as:

$$\alpha^2(a) = \{2\sum_{i=1}^{N} a_{it(i)} \sum_{i=1}^{N} \varphi_i \sum_{i=1}^{N} a_{it(i)}\varphi_i - (\sum_{i=1}^{N} a_{it(i)})^2 \sum_{i=1}^{N} \varphi_i^2 - N(\sum_{i=1}^{N} a_{it(i)}\varphi_i)^2\}$$

$$/\{\sum_{i=1}^{N} a_{it(i)}^2[(\sum_{i=1}^{N} \varphi_i)^2 - N\sum_{i=1}^{N} \varphi_i^2]\} \quad , \tag{3}$$

where N is the number of traces, $a_{it(i)}$ is the amplitude at the i-th trace at two way time t(i) and t(i) lies along the trial stacking hyperbola, ϕ_i are $\sin^2\theta_i$ and θ_i are the reflection angles. Examples in this paper were calculated using the offsets instead of the angles. Also, relating the offset and reflection angle can be done by ray tracing or any other approximations. On the other hand, semblance (NE) which is the normalized output energy of the stack to the gate input energy ratio is given by (Neidell and Taner, 1971):

$$NE = (1/N)\sum_{i=1}^{N} t(\sum_{i=1}^{N} a_{i,t(i)})^2 / \sum_{i=1}^{N} t\sum_{i=1}^{N} a_{it(i)}^2 \quad , \tag{4}$$

where N is the number of traces in the CMP gather, t is the time gate of semblance that follows the path corresponding to the trial stacking hyperbola across the CMP gather, and $a_{i,t(i)}$ is the amplitude value on the i-th trace at the two way time of t(i) where t(i) lies along the trial stacking hyperbola.

The focal transform

The focal transform was introduced by Berkhout et al. (2004) and Berkhout and Verschuur, (2006) as a promising method in the seismic data processing to allow the incorporation of the macro information about the involved wave fields. Application of the focal transform introduces a new domain, the -focal domain- which enables to accurately separate different events from each other. Forward and inverse focal transforms can be formulated as a matrix multiplication per temporal frequency as follows:

$$\mathbf{Q} = \mathbf{FP} \quad , \tag{5}$$

$$\mathbf{P} = \mathbf{GQ} \quad , \tag{6}$$

$$\mathbf{F} = \mathbf{G}^{-1} \quad , \tag{7}$$

where **Q** represents the focal domain, **F** is the inverse operator, **P** represents any prestack 3D data volume with one column representing one monochromatic shot record and **G** is a suitable 3D propagation operator. As a result of applying the focal transform with a suitable operator, energy of reflection event in the input CMP gather will be localized on the focal point in the focal domain.

Using the concept of mentioned equations, the following equations in the time domain was applied.

$$\mathbf{q} = \mathbf{fp} \quad , \tag{8}$$

$$\mathbf{p} = \mathbf{gq} \quad , \tag{9}$$

$$\mathbf{f} = \mathbf{g}^{-1} \quad , \tag{10}$$

where, $\mathbf{q}$ represents the focal domain, $\mathbf{f}$ is the inverse operator, $\mathbf{p}$ represents a CMP gather as a matrix with its columns indicating the traces. On the other word, in matrix $\mathbf{p}$ the row direction is equal to the offset axis and the column direction is equal to the time axis. The dimension of matrix $\mathbf{p}$ is equal to the trace numbers and time samples, and $\mathbf{g}$ is a suitable propagation operator with its dimensions equal to the input CMP gather $\mathbf{p}$. All variables in the above equations are matrices. Assume that an input CMP gather has Nt time samples and Nx traces. Then the input data $\mathbf{p}$ is an Nt by Nx matrix. The operator $\mathbf{g}$ is an Nt by Nx matrix and consequently the inverse operator $\mathbf{f}$ is an Nx by Nt matrix. The matrix $\mathbf{q}$ that is computed by [eq. (8)] is an Nx by Nx matrix where the focal domain $\mathbf{q}$ is always a square matrix. Thus, the forward and inverse focal transformations can be formulated as a matrix multiplication. Using a weighted least-squares inversion approach, the forward focal operator can be written as

$$\mathbf{f} \approx \mathbf{g}^{H}[\mathbf{g}\mathbf{g}^{H} + \varepsilon^{2}\mathbf{I}]^{-1} = \mathbf{g}^{H}\mathbf{b} \quad , \tag{11}$$

$$\mathbf{b} = [\mathbf{g}\mathbf{g}^{H} + \varepsilon^{2}\mathbf{I}]^{-1} \quad , \tag{12}$$

$$\mathbf{q} = \mathbf{g}^{H}\mathbf{bp} \quad , \tag{13}$$

where, $\mathbf{g}^{H}$ is the transpose of $\mathbf{g}$, ε is a small stabilization constant, $\mathbf{I}$ is the unitary matrix and $\mathbf{q}$ represents the focal domain. In the focal transform, the operator $\mathbf{g}$ will be a matrix with the same size and geometry as the input data (the number of rows is equal to the number of samples in the time direction and the number of columns is equal to the number of traces). The focal domain data - if perfectly focused - is mapped along a cross-like event centered in the origin and the slopes of this cross are related to the velocity error in the operator. On the other hand as the focal domain is a square matrix in the perfect case (the operator is the same as the input data) the data is mapped on diagonals of the focal domain. Thus any event in the t-x domain can be localized in the focal domain on the main diagonals by using a proper operator in the transform. This proper operator should be similar to the desired event. Therefore, the reflection events in common midpoint gathers (CMP) can be localized on the main diagonals in the focal domain using a proper operator. The main difference of this formulation with the focal transform introduced by Berkhout and Verschuur

(2006) is that in the optimum case an event is localized on the diagonals instead of the focal point. Therefore, the trend of event amplitudes in the focal domain can be used in the computation of the velocity attribute. The amount of this localization strongly depends on the operator being used in the forward transform. Fig. 1 illustrates how different operators (Figs. 1b, d and f) affect the localization of a single hyperbolic (Fig. 1a) event in the focal domain (Figs. 1c, e, and g). Fig. 1d shows the operator containing a reflecting event similar to the reflecting event in the CMP gather in Fig. 1a. The results of converting the CMP gather in Fig. 1a to the focal domain using the operator in Fig. 1d is shown in Fig. 1e. It can be seen that in cases where the focal operator is equal

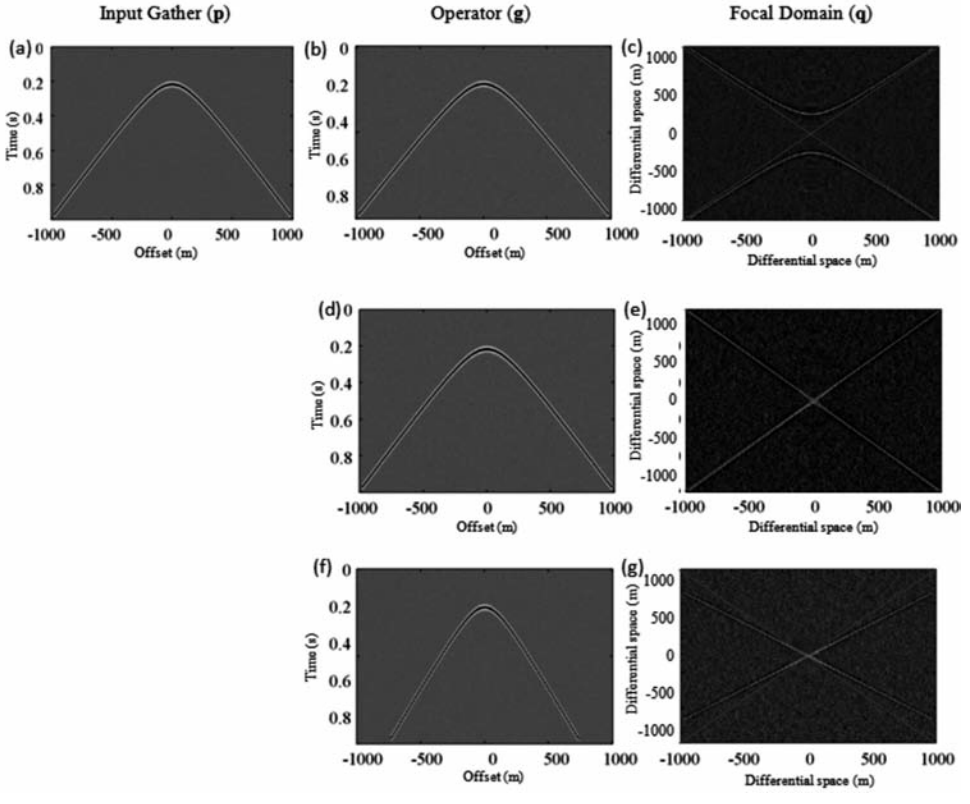

Fig. 1. Illustration of operator effects on the localization of a single hyperbolic event in the focal domain. (a) Synthetic CMP gather containing a reflection event. (b) Single reflection operator; the depth of reflection is shallower than the input CMP gather. (c) Result of applying operator (b) to the input CMP gather. (d) Single reflection operator; the reflection is similar to the input CMP gather. (e) Result of applying operator (d) to the input CMP gather. (f) Single reflection operator; the velocity of the reflection is slower than the input CMP gather. (g) Result of applying operator (b) to the input CMP gather.

to the input CMP gather, an event in the input CMP gather will be moved to the diagonals in the focal domain (red lines in the focal domain). To study the effect of converting the CMP gather to the focal domain with an operator not equal to the input data, two different operators were produced. Fig. 1f shows an operator containing a reflection event with a velocity lower than the velocity of the event in the input CMP gather. Fig. 1g shows the results of converting the CMP gather in Fig. 1a to a focal domain using the operator in Fig. 1f. It is obvious that by using such an operator, in which the event will not move to the main diagonals (red lines in the focal domain). The next test was an operator which contained a reflection event in a shallower depth (Fig. 1b). By applying this operator, the event in the CMP gather was not moved to the diagonals either (red lines in the focal domain, Fig. 1c). Therefore, high amplitude values on the diagonals of the focal domain can be obtained only if the operator has an event similar to the event in the input CMP gather.

AB Focal Velocity Analysis (*AB*-FVA)

Velocity analysis in the focal domain is based on the fact that the location of an event in the focal domain strongly depends on the operator being used in the focal transform. In the case the event in the operator is equal to one of the events in input CMP gather, that event will be mapped onto the main diagonals of the focal domain. On the other hand, even small differences between the operator event and the events in the input gather lead to mapping that event onto other areas. Considering the above concept, the generalized semblance measurement [eq. (3)] of the main diagonals of the focal domain can be used as a velocity attribute in a velocity analysis. Since the generalized semblance measurement is the main equation in generation of the *AB* semblance and the velocity attribute of this method used the same equations, this method is called *AB*-FVA (*AB* Focal Velocity Analysis).

Fig. 2 shows the flowchart of applying an *AB*-FVA. On each iteration for the velocity V_i and time T_j, an operator containing a reflection event with V_{rms} equal to V_i and apex time equal to T_j will be generated. The generation of the operators can be done by using ray tracing or any other method that can generate gathers which contain a reflection event with the mentioned parameters. Then, the focal domain of the input CMP gather will be calculated using the generated operator. In the next step, the correlation coefficient ($a_{i,j}$) of the diagonals in the focal domain will be calculated by using a generalized semblance measurement [eq. (3)]. The above-mentioned procedures shall be repeated for all velocities and times. The Final velocity panel will be generated by plotting $a_{i,j}$ for all i and j values side by side. The main difference between the FVA and *AB*-FVA is using the generalized semblance measurement [eq. (3)] instead of simple summation. Since this measurement [eq. (3)] uses the Shuey's approximation [eq. (1)] as a trend, it can involve the term of amplitude variation

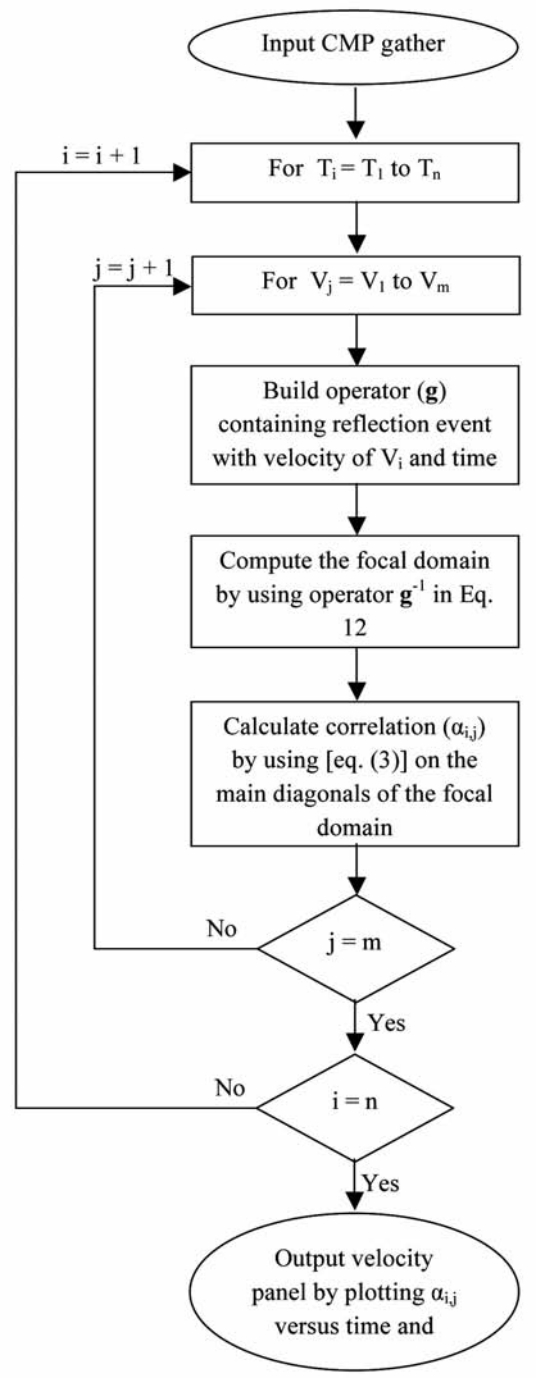

Fig. 2. The flowchart of applying an *AB*-FVA. The difference between FVA and *AB*-FVA is using a generalized semblance measurement [eq. (3)] instead of simple summation in focal velocity analysis.

versus angle in measurements. So, by using this measurement, *AB*-FVA can involve the effect of AVO anomalies in calculations. In the absence of the trend (set the B equal to zero in [eq. (1)]) the generalized semblance measurement [eq. (3)] will change to common semblance [eq. (4)].

Fig. 3 shows the schematic view of the above procedures. Fig. 3a shows a schematic CMP gather containing one reflection event. Fig. 3b is the schematic view of three sample operators of all operators. By computing the focal domain using operators on Fig. 3b, the focal domains were obtained (Fig. 3c). Calculating the correlation coefficient ($a_{i,j}$) with the generalized semblance measurement [eq. (3)] on the main diagonals of the focal domain results in ($a_{i,j}$). Plotting all ($a_{i,j}$) beside each other lead to the velocity panel in Fig. 3d.

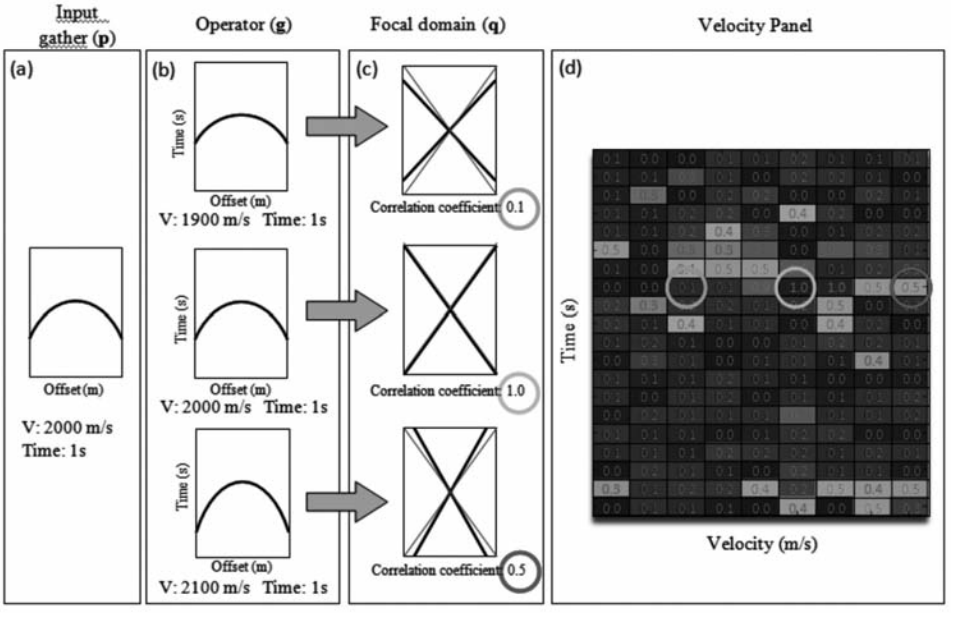

Fig. 3. A schematic diagram showing a focal-transform velocity analysis methodology. (a) Schematic view of the input CMP gather containing a reflection event with a velocity of 2000 m/s and apex time of 1 s. (b) Schematic view of three of operators used in a focal transform built to contain a reflection event with velocities equal to 1800 m/s, 2000 m/s and 2100 m/s, respectively. (c) Schematic view of a focal domain related to each of the mentioned operators. Correlation coefficient of diagonals (indicated by a red cross) of each focal domain calculated by generalized semblance measurement [eq. (3)] and shown in colored circles. By substituting [eq. (3)] with simple summation of amplitudes, *AB*-FVA is converted to FVA. (d) Velocity panel of the input CMP gather is obtained by putting correlation coefficient values (from focal domains) side by side for different times and velocities. The value of each pixel in the velocity panel matrix calculated from an operator containing the reflection event with velocities and times related to that pixel in the velocity panel. Three of these operators are shown in (b) and related pixels in the velocity panel are marked with color circles.

EXAMPLES

Synthetic

Two sets of synthetic data were generated to demonstrate the results from an *AB*-FVA and their comparison with other methods. The first dataset was a horizontally layered medium with two interfaces (Fig. 4a). In this model, layers were defined with the Poisson's ratios of 0.4, 0.1 and 0.4 for the upper, middle, and lower layers respectively as:

$$\alpha_2/\alpha_1 = \alpha_3/\alpha_2 = \rho_2/\rho_1 = \rho_3/\rho_2 = 1.11 \quad , \tag{14}$$

where a_1, a_2 and a_3 are the velocity of the first, second and third layers, respectively, also ρ_1, ρ_2 and ρ_3 are the density of the first, second and third layers, respectively. The Synthetic CMP gather was generated using the ray-tracing algorithm in the mentioned model for every 50 m traces. Fig. 4b shows the results of ray tracing after convolution with a minimum phase Ricker wavelet with sample interval of 4 ms. It can be seen both interfaces show a class

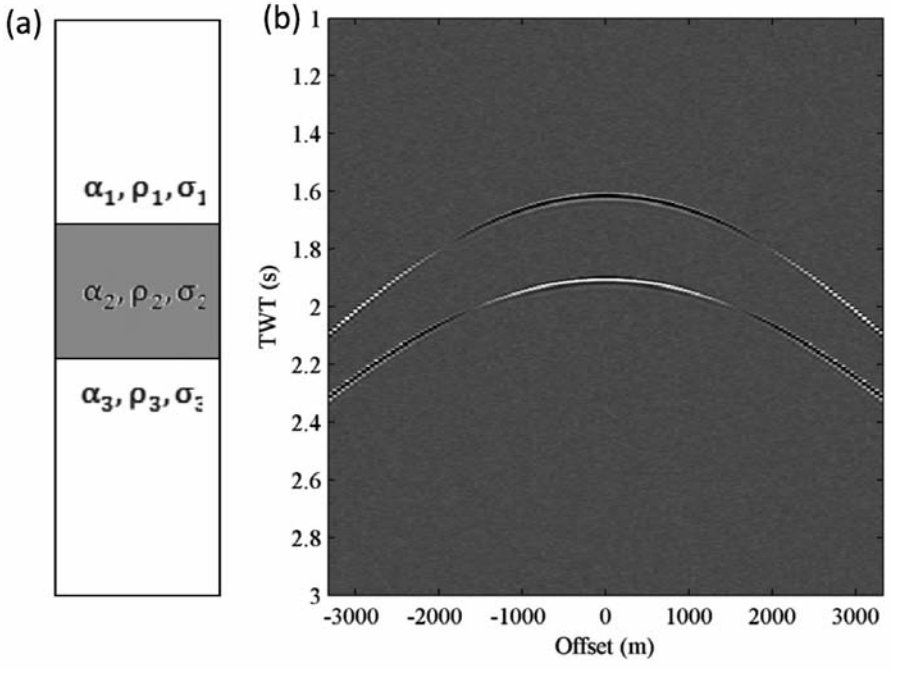

Fig. 4. Synthetic CMP gather of horizontally layered media with two interfaces. In this model, the layers were defined with the Poisson ratios of 0.4, 0.1 and 0.4 for the upper, middle, and lower layers, respectively. (a) Schematic view of the model. (b) The synthetic CMP gather was generated by using the ray tracing algorithm in the mentioned model. Sampling interval is 4 ms and trace interval is 50 m. The results of ray tracing after convolution with a minimum-phase Ricker wavelet are shown in this figure.

2 AVO anomaly. Fig. 5 shows the results of applying the semblance, *AB* semblance, focal and *AB*-FVA. All velocity analysis was run with a time interval of 4 ms and a velocity interval of 5 m/s. To assess the results of these methods, four sections with a constant velocity and eight sections with constant times were generated which are shown in Figs. 6 and 7, respectively. Fig. 6 shows four sections at the velocity of 2500 m/s which is the true velocity of the upper layer. In this Figure, the exact time of reflections were indicated by dashed red lines. By defining a higher resolution as a narrower peak, it can be concluded that both focal (Fig. 6c) and *AB*-FVA (Fig. 6d) can locate reflection events more accurately and with a higher resolution than the two other methods. Fomel (2009) mentioned that the *AB* semblance had a lower resolution than the semblance as it can be seen in Figs. 6a and 6b.

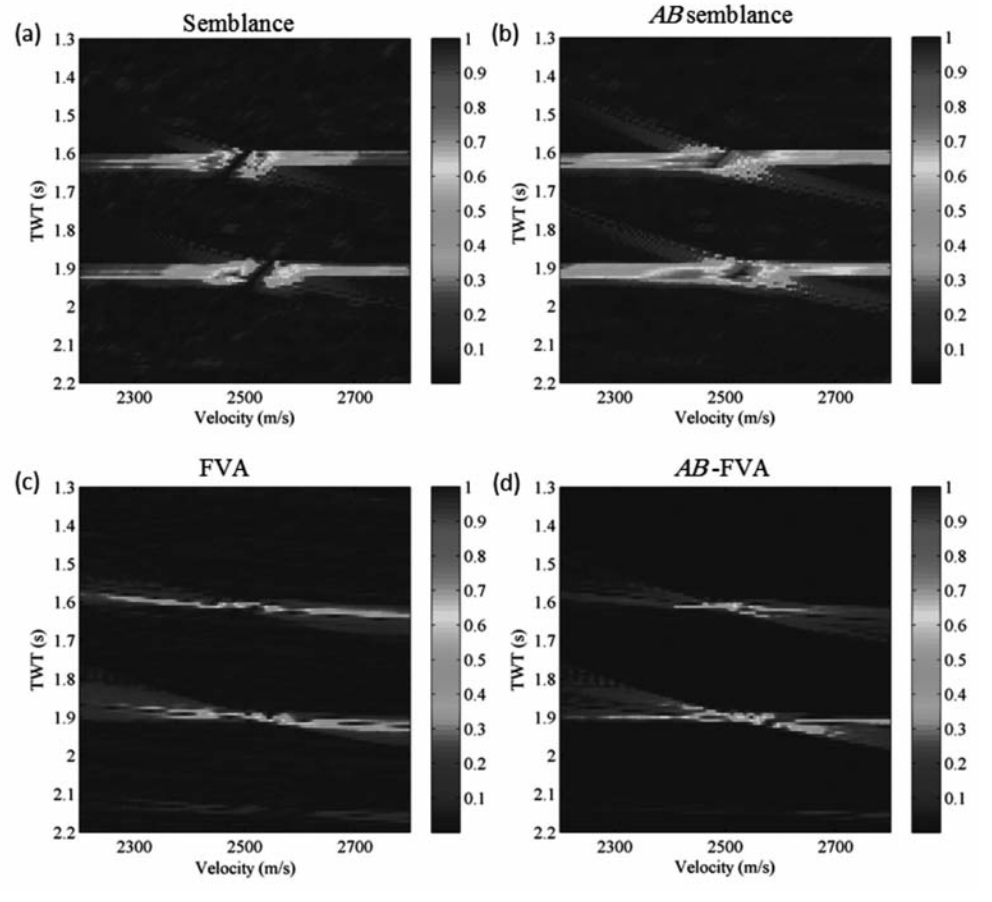

Fig. 5. Velocity analysis of synthetic data in Fig. 4 by (a) semblance, (b) *AB* semblance, (c) FVA and (d) *AB*-FVA. Time sampling in velocity analysis is 4 ms and velocity sampling is 5 m/s.

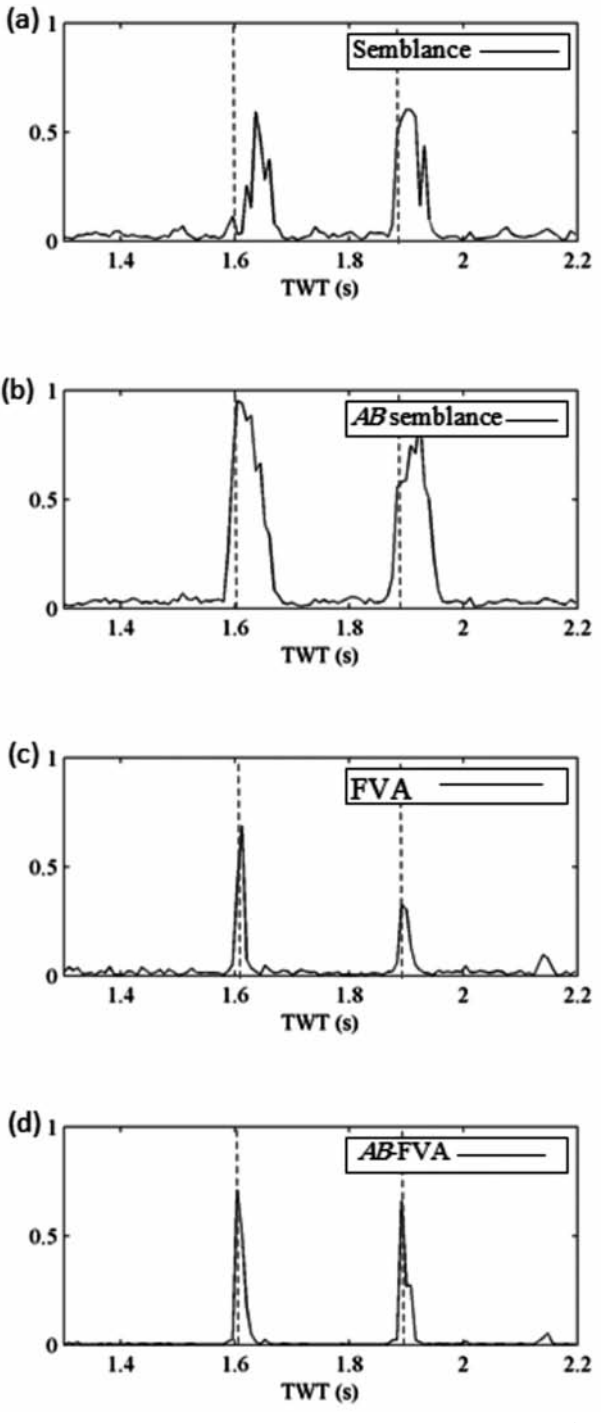

Fig. 6. Four velocity slices with a constant velocity of 2500 m/s from Fig. 5. (a) Semblance, (b) *AB* semblance, (c) FVA and (d) *AB*-FVA.

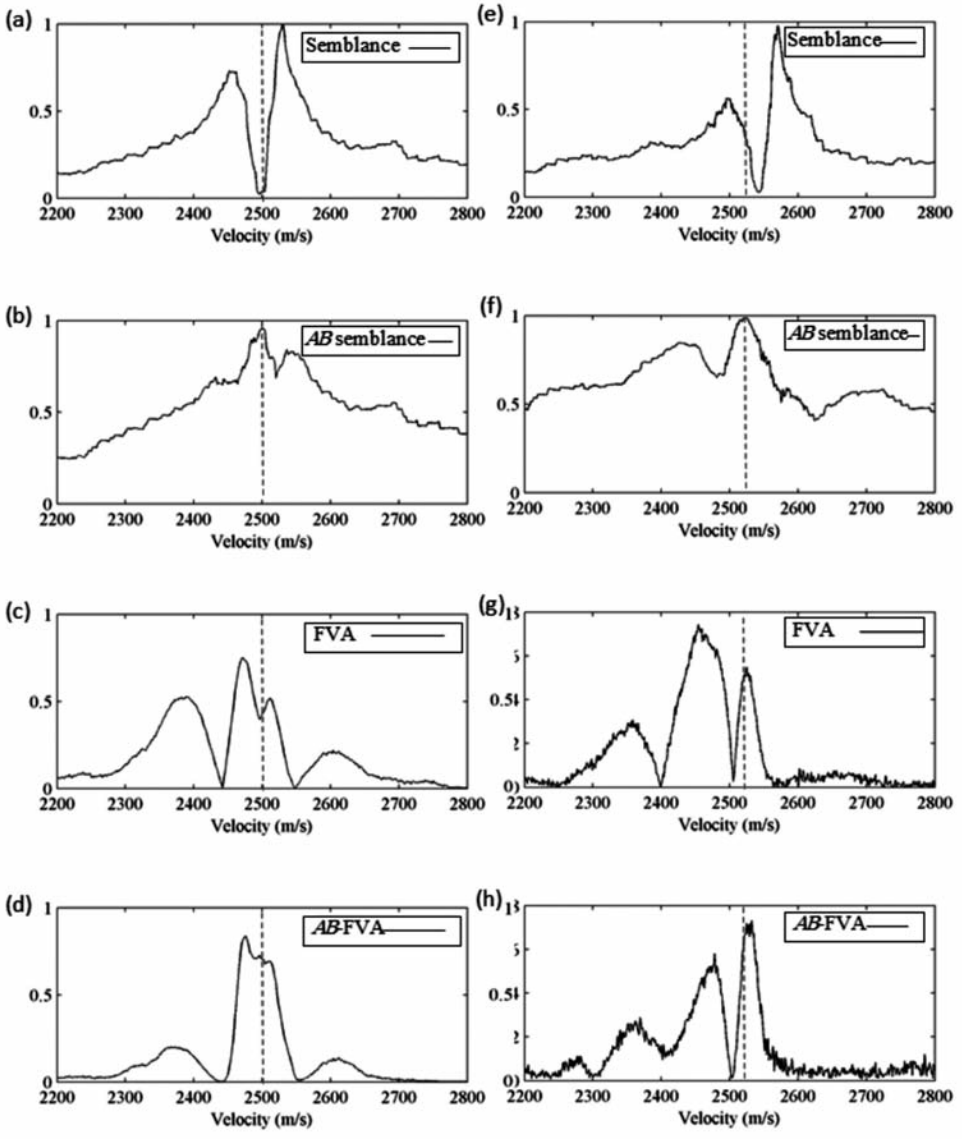

Fig. 7. Eight sections with constant times of 1.6 s and 1.9 s from Fig. 5. (a) Semblance, (b) *AB* semblance, (c) FVA and (d) *AB*-FVA at time 1.6 s. (e) Semblance, (f) *AB* semblance, (g) FVA and (h) *AB*-FVA at time 1.9 s.

Fig. 7 shows eight sections at the times of 1.6 s and 1.9 s which are the true times of reflections as in Fig. 5. In Fig. 7, the true velocities of events are indicated by red dashed lines. The most noticeable phenomena in this Figure are that the semblance (Fig. 7b) and focal (Fig. 7c) do not show a peak at the true velocity of the events. This is the pitfall of those methods that assume no amplitude variation with the offset. Therefore, as both reflections in this dataset show the class 2 AVO anomaly, this effect can be seen. This pitfall can be overcome by taking the AVO effects into account using a generalized semblance measurement as the one used in both *AB* semblance and *AB*-FVA velocity analysis. Figs. 7b and 7d show that both *AB* semblance and *AB*-FVA can correctly indicate the velocities of the events. Also, since the *AB*-FVA results have a narrower peak in both time and velocity directions, it can be concluded that the *AB*-FVA has a higher resolution in comparison with the *AB* semblance.

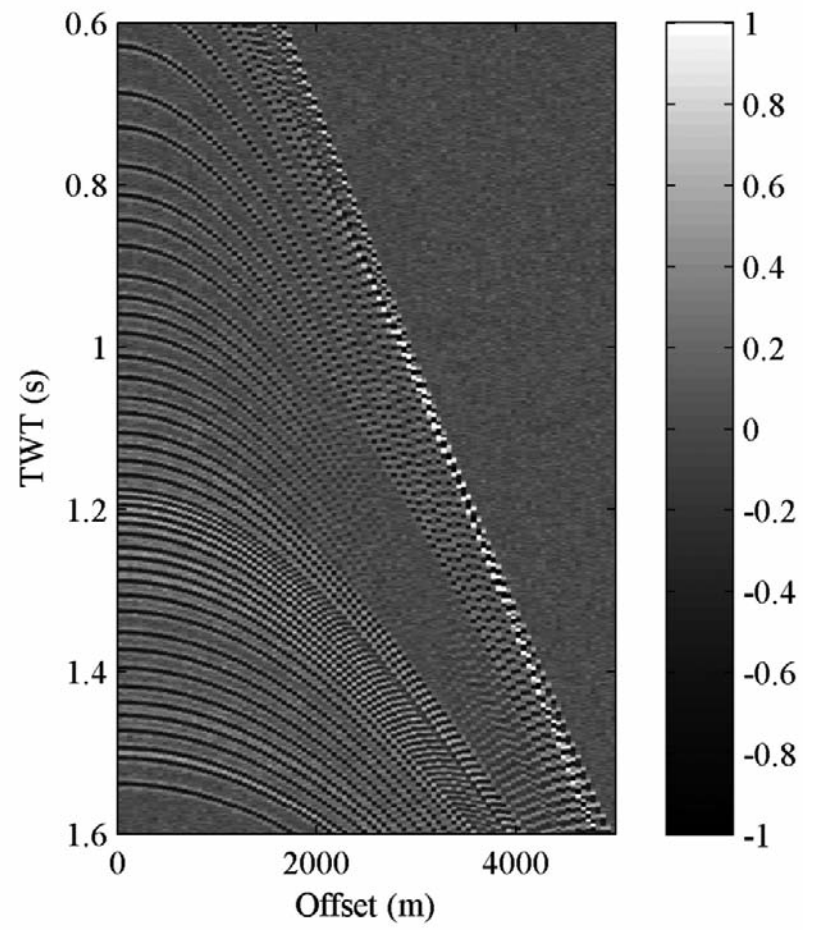

Fig. 8. Synthetic data containing many reflections with a sampling interval of 4 ms and a trace interval of 50 m.

The second synthetic dataset was generated by convolving a random time series as the times of reflections with zero-phase Ricker wavelet with a dominant frequency of 40 Hz and a reasonable interval of P-wave velocities. To assess the four mentioned methods, only a class 2 AVO anomaly was added to the reflections between 0.9 to 1.1 s (Fig. 8). Fig. 9 shows the results of applying the velocity analysis to Fig. 8. This Figure demonstrates that the *AB* semblance shows much smearing in comparison with the others, whereas the *AB*-FVA shows the least smearing in time and velocity directions. Similar to the previous model, four sections with a constant velocity of 3400 m/s were produced for the assessment of the methods (Fig. 10). This velocity was equal to the velocity of one of the reflection events that showed an AVO anomaly. The region of this event on the velocity panels is indicated by a red box in Fig. 9. As it is clear in Fig. 10, the semblance (Fig. 10a) and the focal (Fig. 10c) methods are not able to locate the exact time of this event correctly (the exact time of the event is indicated by the dashed red line). On the other hand, the *AB* semblance (Fig. 10b) and *AB*-FVA (Fig. 10c) results can clearly locate the mentioned event. It can also be seen that *AB*-FVA has a higher resolution and lower smearing in comparison with the *AB* semblance. Fig. 11 shows four the sections with a constant time equal to .95 which is the time of the event studied in the previous figure (indicated by a red box in Fig. 9). As it is clear, the semblance (Fig. 11a) and focal (Fig. 11c) results suffer from the same pitfall in Fig. 7 and this pitfall has been overcome in *AB* semblance (Fig. 11b) and *AB*-FVA (Fig. 11d) results. In addition, it is noticeable that the *AB*-FVA has a narrower peak and accordingly a higher resolution. Also, in comparison with other velocity analysis methods, it can be seen that the *AB*-FVA has lower background noise.

Field data

Two sets of real data were used to demonstrate the results from *AB*-FVA on field data and also to compare the results with the three other methods. The first dataset was offshore data that contained long period multiples (Fig. 12). This data was deep marine acquisition that contained strong multiple events that started at two way time 1.3 s. Figs. 13 and 14 show the results of applying semblance, *AB* semblance, FVA and *AB*-FVA. It can be seen that *AB* semblance and *AB*-FVA show larger smearing in comparison with semblance and FVA, respectively. Besides this, FVA and *AB*-FVA have higher resolution (especially in time direction) in comparison with the semblance and the *AB* semblance. The second dataset was the shallow part of a CMP gather that showed class 2 AVO anomaly at time 350 ms after NMO correction (Fig. 15). Fig. 16 shows the results of applying residual velocity analysis with the method of semblance and *AB* semblance. Furthermore, Fig. 17 shows the results of applying residual velocity analysis with the method of FVA and *AB*-FVA. The results show that *AB* semblance and *AB*-FVA can show a better velocity analysis at the time of the event with the AVO anomaly. Also, FVA and *AB*-FVA have higher resolution in comparison with the other two methods.

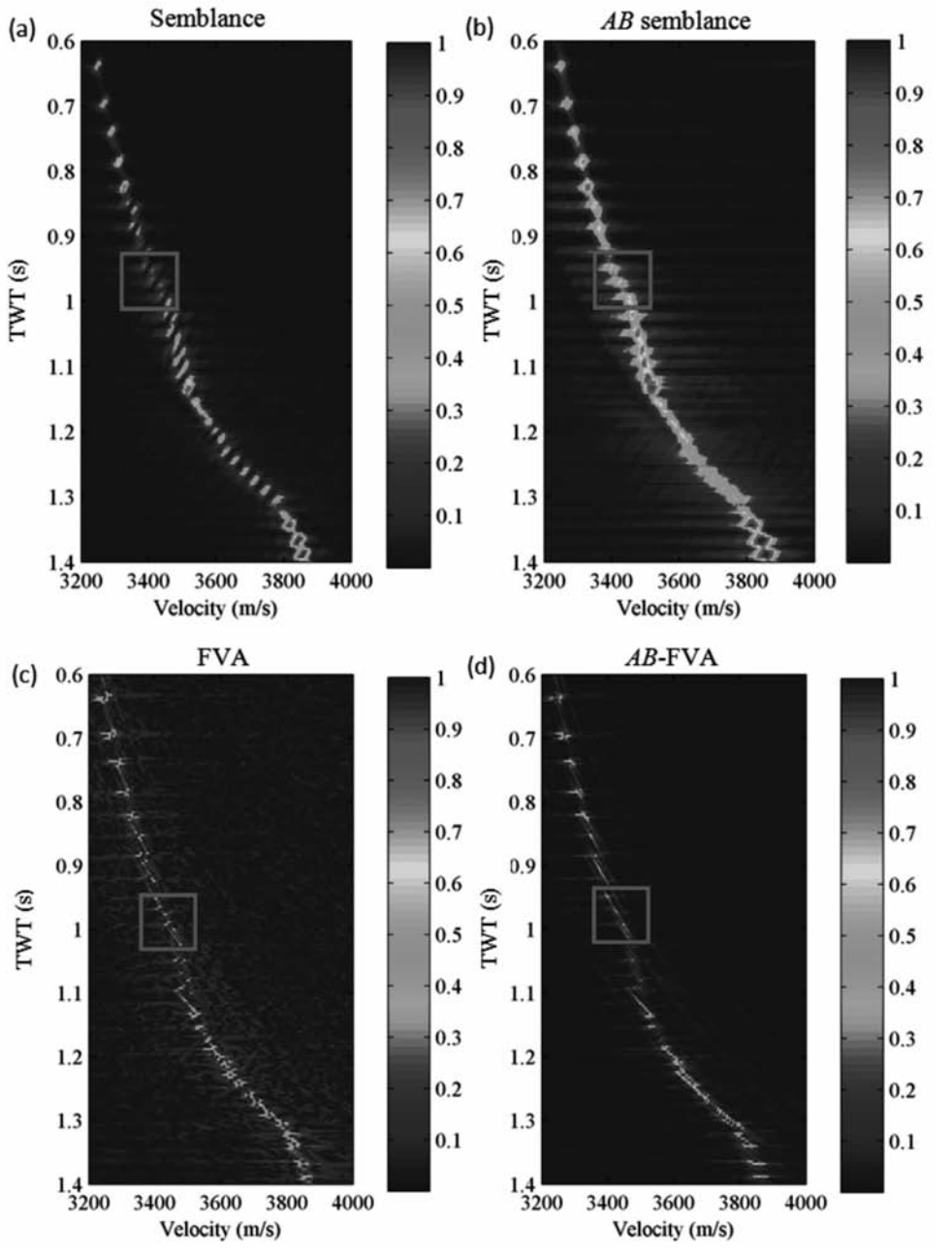

Fig. 9. Velocity analysis of the synthetic data in Fig. 8 by (a) semblance, (b) *AB* semblance, (c) focal and (d) *AB*-FVA. Time sampling in velocity analysis is 4 ms and velocity sampling is 5 m/s.

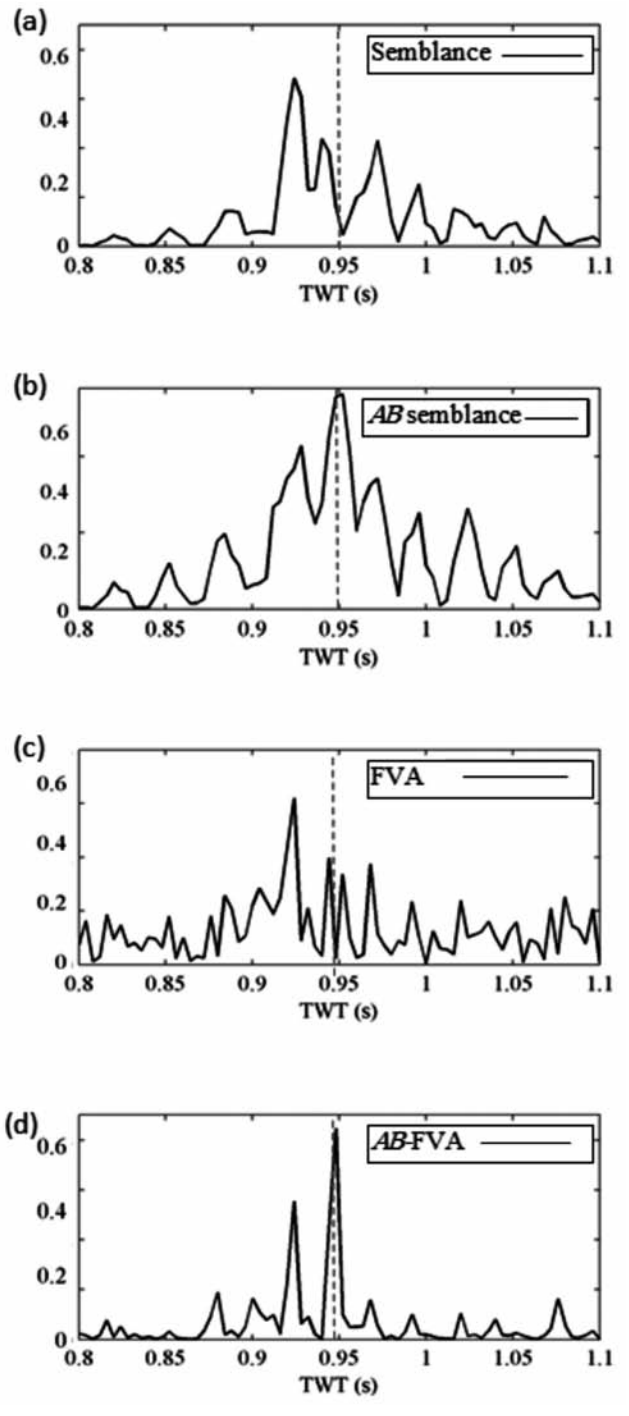

Fig. 10. Four sections with a constant velocity of 3400 m/s from the velocity panel from Fig. 9. (a) Semblance, (b) *AB* semblance, (c) FVA and (d) *AB*-FVA.

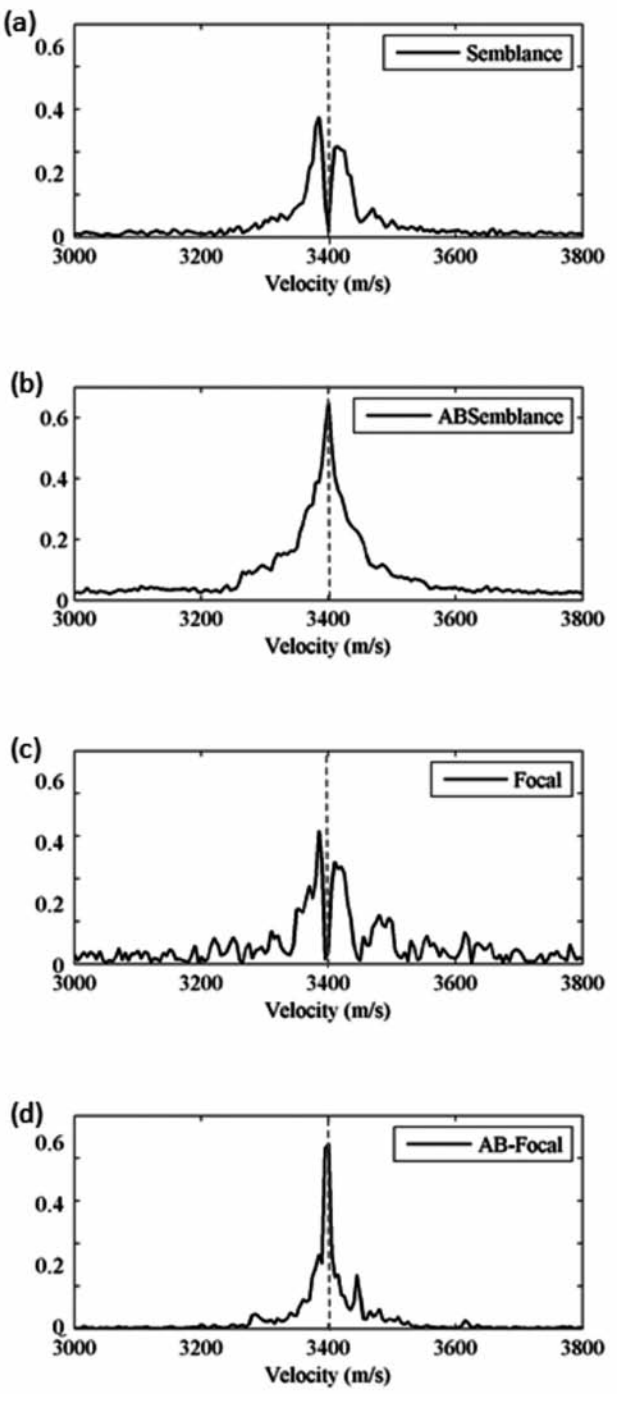

Fig. 11. Four sections with a constant time of 0.95 s from Fig. 9. (a) Semblance, (b) *AB* semblance, (c) FVA and (d) *AB*-FVA.

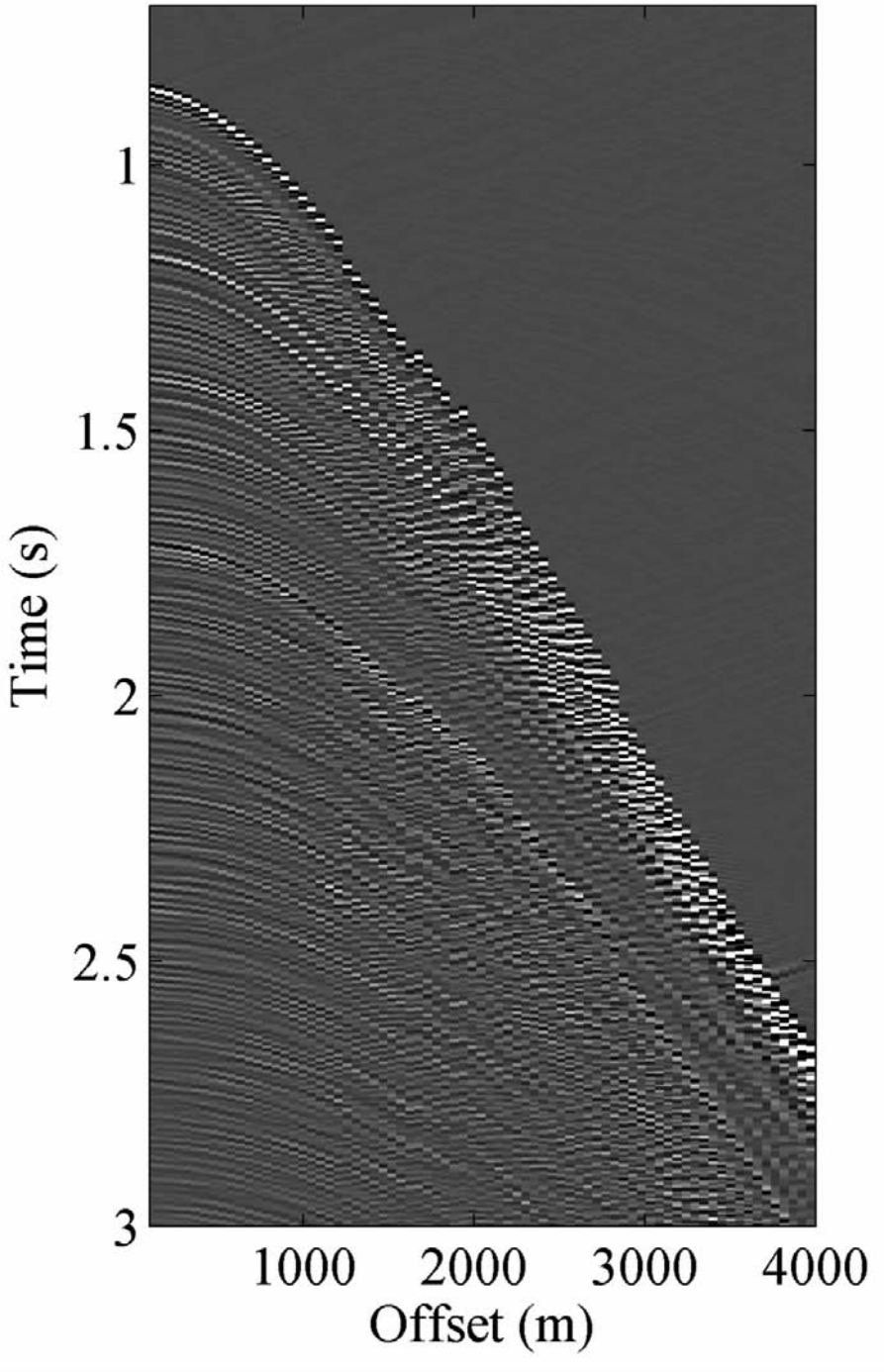

Fig. 12. A marine CMP gather containing long period multiples with a sample interval of 2 ms and a trace spacing of 50 m.

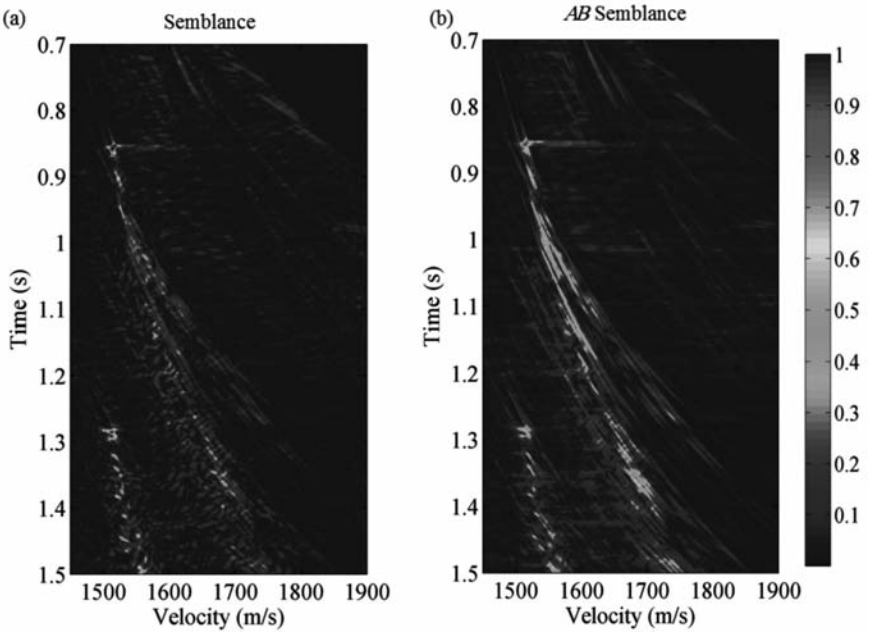

Fig. 13. Velocity analysis with a time sampling of 2 ms and a velocity sampling of 5 m/s of the CMP gather in Fig. 12. (a) semblance and (b) *AB* semblance.

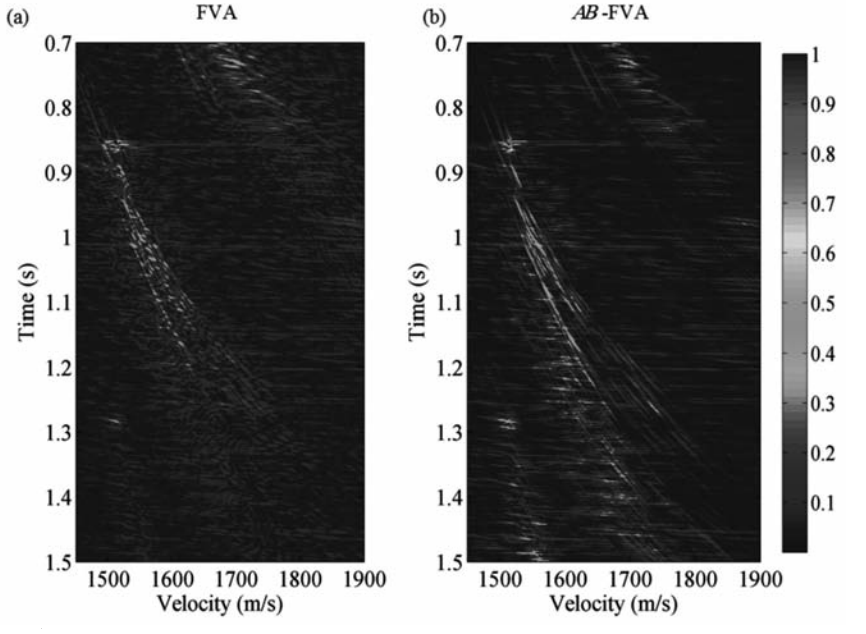

Fig. 14. Velocity analysis with a time sampling of 2 ms and velocity sampling of 5 m/s of the CMP gather in Fig. 12. (a) FVA and (b) *AB*-FVA.

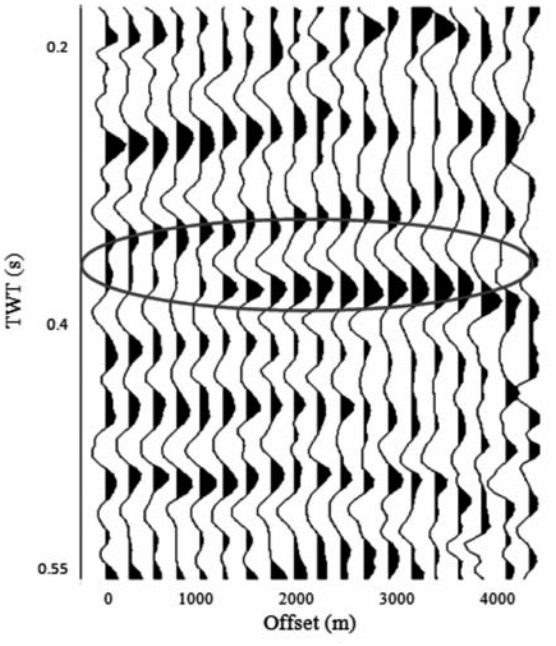

Fig. 15. A CMP gather that shows the class 2 AVO anomaly with a sample interval of 4 ms.

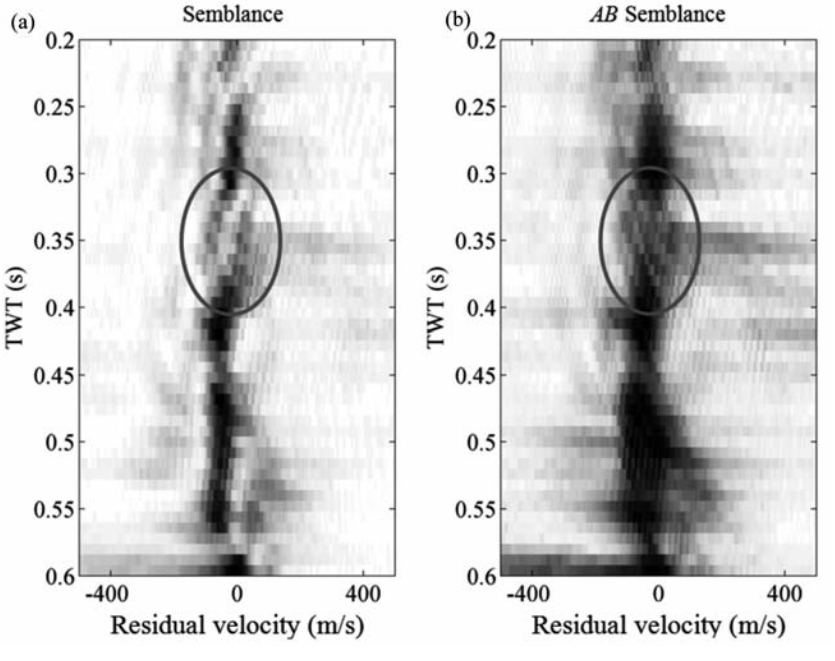

Fig. 16. Velocity analysis with a time sampling of 4 ms and a velocity sampling of 5 m/s of the CMP gather in Fig. 15 containing class 2 AVO . (a) Semblance and (b) *AB* semblance.

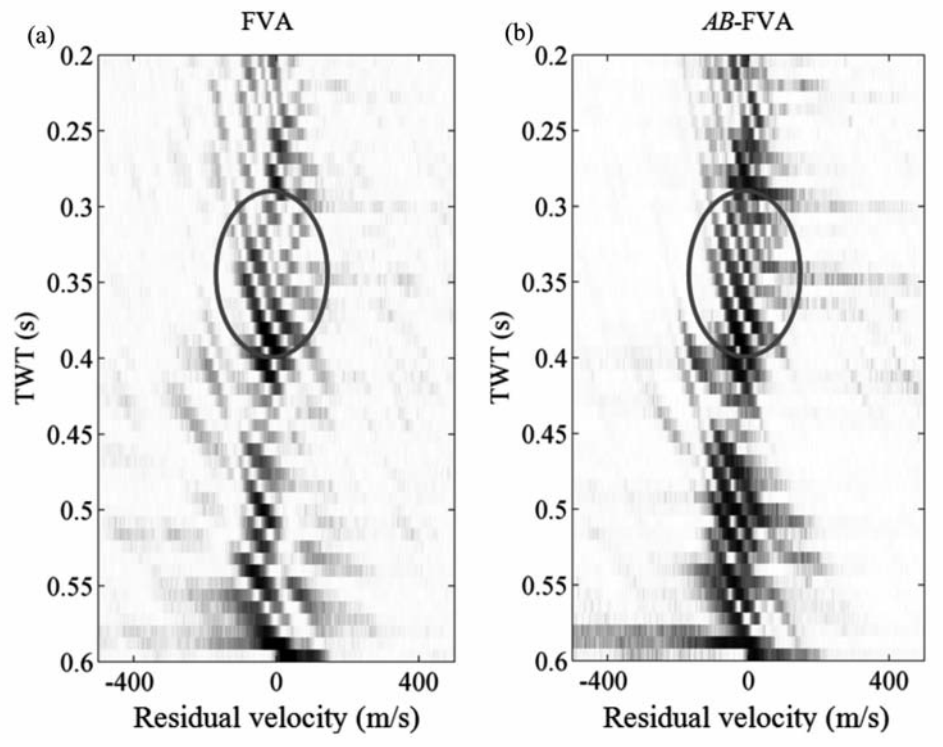

Fig. 17. Velocity analysis with a time sampling of 4 ms and velocity sampling of 5 m/s of the CMP gather in Fig. 15 containing class 2 AVO. (a) FVA and (b) *AB*-FVA.

CONCLUSIONS

According to the results of applying the *AB*-FVA and other three methods to the velocity analysis for two synthetic CMP gathers, it was concluded that the *AB*-FVA and *AB* semblance enable us to handle the class 2 AVO effect of the reflection events in a velocity analysis. A comparison of the results of the velocity analysis obtained by the *AB*-FVA with those obtained by the *AB* semblance demonstrated that a high resolution velocity analysis in both time and velocity directions were achieved by using the focal domain. Also, it was observed that the *AB*-FVA had lower background noise and smearing in comparison with the others.

ACKNOWLEDGMENTS

The authors would like to thank D.J. Verschuur for his constructive comments and useful suggestions to improve this paper. Also, the authors would like to thank the editorial office of this journal.

REFERENCES

Berkhout, A.J. and Verschuur, D.J., 2006. Focal transformation, an imaging concept for signal restoration and noise removal. Geophysics, 71: A55-A59.

Berkhout, A.J., Verschuur, D.J. and Romijn, R., 2004. Reconstruction of seismic data using the focal transformation. Expanded Abstr., 74th Ann. Internat. SEG Mtg., Denver: 1993-1996.

Biondi, B.L. and Kostov, C., 1989. High resolution velocity spectra using eigenstructure methods. Geophysics, 54: 832-842.

Fomel, S., 2009. Velocity analysis using *AB* semblance. Geophys. Prosp., 57: 311-321.

Key, S.C. and Smithson, S.B., 1990. A new method of event detection and velocity estimation. Geophysics, 55: 1057-1069.

Neidell, N.S. and Taner, M.T., 1971. Semblance and other coherency measures for multichannel data. Geophysics, 36: 482-497.

Rutherford, S.R. and Williams, R.H., 1989. Amplitude-versus-offset variations in gas sands. Geophysics, 54: 680-688.

Sarkar, D., Baumel, R.T. and Larner, K.L., 2002. Velocity analysis in the presence of amplitude variation. Geophysics, 67: 1664-1672.

Sarkar, D. Castagna, J.P. and Lamb, W.J., 2001. AVO and velocity analysis. Geophysics, 66: 1284-1293.

Shuey, R.T., 1985. A simplification of the Zoeppritz-equations. Geophysics, 50: 609-614.

Symes, W.W. and Kern, M., 1994. Inversion of reflection seismograms by differential semblance analysis: algorithm structure and synthetic examples. Geophys. Prosp., 42: 565-614.

Torabi, S. and Javaherian, A. 2010. Introducing a new method in velocity analysis by using focal transform. Expanded Abstr., 72th EAGE Conf., Barcelona: P392.

Torabi, S., Javaherian, A. and Nabi-Bidhendi, M. 2013. Velocity analysis by focal transform. J. Seismic Explor., 22: 373-388.